I&EC research
Industrial & Engineering Chemistry Research

Article

pubs.acs.org/IECR

Atomically Detailed Modeling of Metal Organic Frameworks for Adsorption, Diffusion, and Separation of Noble Gas Mixtures

Yeliz Gurdal and Seda Keskin*

Department of Chemical and Biological Engineering, Koç University, Rumelifeneri Yolu, Sariyer, 34450, Istanbul, Turkey

Supporting Information

ABSTRACT: Atomically detailed simulations have been widely used to assess gas storage and gas separation properties of metal organic frameworks (MOFs). We used molecular simulations to examine adsorption, diffusion, and separation of noble gas mixtures in MOFs. Adsorption isotherms and self-diffusivities of Xe/Kr and Xe/Ar mixtures at various compositions in ten representative MOFs were computed using grand canonical Monte Carlo and equilibrium molecular dynamics simulations. Several properties of MOFs such as adsorption selectivity, working capacity, diffusion selectivity, permeation selectivity, and gas permeability were evaluated and compared with those of traditional nanoporous materials. Results showed that MOFs are promising candidates for Xe/Kr and Xe/Ar separations due to their high Xe selectivity and permeability.

INTRODUCTION

Metal organic frameworks (MOFs) are a new class of nanoporous materials that are comprised of self-assembly of metal ions which act as coordination centers and organic ligands which act as linkers between metal centers. MOFs have been attracting academic and industrial attention due to their interesting chemical and physical properties such as high porosities, large surface areas, low densities, high gas uptake capacities, and wide range of pore sizes. With these properties, MOFs have been considered to be promising materials in a variety of applications including gas storage, gas separation, catalysis, and chemical sensing. The greatest advantage of MOFs over well-known traditional nanoporous materials is the ability to tune their physical and chemical properties during synthesis. Thousands of distinct MOF materials have been synthesized to date,[1−5] and a theoretically infinite number of materials can be synthesized by changing the combination of metals and organic linkers. Since the number of MOFs that has been synthesized is enormous, molecular modeling of these materials has played an important role in providing information about the performance of MOFs for specific applications.[6−8]

MOFs have been widely studied for gas storage and gas separation. A large number of molecular simulation studies investigated adsorption of CO_2, CH_4, N_2, and H_2 in addition to separation of CO_2/CH_4, CH_4/H_2, CO_2/N_2, and CO_2/H_2 mixtures using grand canonical Monte Carlo (GCMC) simulations. For example, Krishna and van Baten[9,10] studied MOFs and zeolite imidazolate frameworks (ZIFs) for CO_2/CH_4, CH_4/H_2, CO_2/N_2, CO_2/H_2, and hydrocarbon separations. Liu et al.[11] examined MOFs ability to separate CO_2/H_2 and CH_4/H_2 mixtures. Yang and co-workers[12] investigated separation of CO_2 from flue gases using CuBTC. Liu et al.[11] studied separation performances of MOFs and covalent organic frameworks (COFs) for CO_2/CH_4, CH_4/H_2, and CO_2/H_2 mixtures. Guo et al.[13] used molecular simulations for adsorption and separation of CH_4/H_2 mixtures in ZIFs. Jiang's group[14−18] studied adsorption of CO_2 and CO_2/CH_4 mixtures in ZIFs, bioMOFs, and catenated, metal-exposed, and charged MOFs. Keskin et al.[19−24] examined separation performances of isoreticular MOFs (IRMOFs), bioMOFs, CPOs (coordination polymers of Oslo), ZIFs and COFs for CO_2/CH_4, CH_4/H_2, and CO_2/H_2 mixtures.

In contrast to the high number of molecular simulation studies for separation of CO_2, CH_4, N_2, and H_2, only very few publications addressed capture and separation of noble gases using MOFs.[25−28] Noble gas separation plays a significant role in industry since these gases have specific properties such as the lack of chemical reactivity, low solubility, very low conductivity, very low boiling, and melting points. For example, Xe has several usage including lighting, imaging, anesthesia, nuclear magnetic resonance, and separation of Xe from Kr is required to obtain high purity Xe. The conventional approach which employs energetically intensive cryogenic distillation to produce pure Xe and pure Kr has been replaced by adsorption-based separation which utilizes nanoporous materials such as zeolites and activated carbon. Development of new materials that can exhibit higher selectivity than traditional zeolites for adsorption-based separation of noble gases is crucial.

To date, there have been only two molecular simulation studies in the literature related to the noble gas adsorption in MOFs. Greathouse et al.[25] used GCMC simulations to report Xe and Ar adsorption in IRMOF-1. They also studied adsorption selectivity of IRMOF-1 for Xe/Ar and Xe/Kr mixtures and concluded that IRMOF-1 can be a promising material for separation of Xe. The second molecular modeling study for noble gas separation was performed by Ryan et al.[26] They used GCMC simulations to obtain single component and mixture adsorption of Xe and Kr in IRMOF-1, HKUST-1, UMCM-1, ZIF-8, MOF-505, NOTT-101, NOTT-108, and Pd-MOF and concluded that large pore materials are not desirable

Received: March 22, 2012
Revised: May 8, 2012
Accepted: May 9, 2012
Published: May 9, 2012

   dx.doi.org/10.1021/ie300766s | Ind. Eng. Chem. Res. 2012, 51, 7373−7382

Table 1. Structural Properties of MOFs Studied in This Work[a]

material	crystal type	a, b, c (Å)	α, β, γ (deg)	pore size (Å)	fractional porosity
BioMOF-11	tetragonal	15.435, 15.435, 22.775	90, 90, 90	5.2, 5.8	0.54
CuBTC	cubic	26.343, 26.343, 26.343	90, 90, 90	3.5, 5, 9	0.72
CPO-27-Co	hexagonal	25.885, 25.885, 6.806	90, 90, 120	11	0.48
CPO-27-Ni	hexagonal	25.785, 25.785, 6.770	90, 90, 120	11	0.48
IRMOF-1	cubic	25.669, 25.669, 25.669	90, 90, 90	10.9, 14.3	0.79
ZIF-1	monoclinic	9.740, 15.266, 14.936	90, 98.62, 90	3, 6.9	0.56
ZIF-2	orthorhombic	9.679, 24.114, 24.45	90, 90, 90	6.4, 6.9	0.66
ZIF-3	tetragonal	18.970, 18.970, 16.74	90, 90, 90	4.6, 6	0.68
ZIF-10	tetragonal	27.061, 27.061, 19.406	90, 90, 90	8.2, 12.1	0.73
$Zn(bdc)(ted)_{0.5}$	tetragonal	14.899, 14.899, 19.136	90, 90, 90	3.2, 4.8, 7.5	0.65

[a]Porosity and free volume values of MOFs were taken from the study of Wu et al.[69] except CPOs and $Zn(bdc)(ted)_{0.5}$ for which values were taken from the works of Dietzel et al.[38] and Liu et al.,[43] respectively.

for efficient adsorption-based separation of Xe/Kr. The number of experimental studies on noble gas storage and separation with MOFs is also very limited. Mueller et al.[4] measured Xe, Kr, and Ar uptake of IRMOF-1 and reported that this MOF exhibits preferential adsorption for Xe over other lighter noble gases. Thallapally et al.[27] recently measured adsorption isotherms of Xe and Kr in CPO-27-Ni (NiDOBDC) and showed that the uptake capacity of CPO-27-Ni is substantially higher than that of IRMOF-1 and similar to that of activated carbon. Hoffmann et al.[28] performed NMR spectroscopic measurements and measured adsorption and desorption of Xe in DUT-8.

In this work, we used atomically detailed modeling methods to examine both single component and mixture adsorption of Xe, Kr, and Ar in ten representative MOFs. We used GCMC simulations and Ideal Adsorbed Solution Theory to compute adsorption of gas mixtures in MOFs. In addition to calculating adsorption selectivities, we also computed self-diffusivities of each component in Xe/Kr and Xe/Ar mixtures using equilibrium molecular dynamics simulations and predicted permeation selectivity of MOFs in noble gas separations for the first time in the literature. The working capacity and gas permeability of each MOF were computed using the data obtained from detailed molecular simulations and performances of MOFs were compared with other nanoporous materials including zeolites and carbon nanotubes. Finally, we discussed which material properties are desirable to develop more selective MOF materials for adsorption-based and membrane-based separation of Xe/Kr and Xe/Ar.

Details of Molecular Simulations. In this study, grand canonical Monte Carlo (GCMC) and equilibrium molecular dynamics (EMD) simulations were used to compute adsorption and diffusion of Xe, Kr, Ar, and their binary mixtures in MOFs. We chose ten MOFs having different metal sites, organic linkers, topologies, and pore sizes to represent a variety of MOF properties. Structural information of MOFs including unit cell parameters and pore sizes are given in Table 1. IRMOF-1, the prototype of isoreticular MOFs, is a three-dimensional cubic structure with pore sizes 10.9/14.3 Å in diameter.[29] It has been very widely studied in the literature for gas adsorption and separation applications.[30−33] Cu-BTC, also known as HKUST-1, has main channels 9 Å in diameter, surrounded by tetrahedral pockets with diameters of 5 Å and windows 3.5 Å wide.[34] Similar to IRMOF-1, CuBTC is one of the most widely examined MOFs for gas storage and separation.[35,36] The CPO-27-M structures (M = Ni, Co) were recently reported; they have three-dimensional structures with honeycomb-like topology that contains a one-dimensional channel in the honeycomb with a diameter of ∼11 Å.[37,38] Zeolite imidazolate frameworks (ZIFs) are a new subclass of MOFs, which have tetrahedral networks that resemble those of zeolites with transition metals linked by imidazolate ligands.[39,40] ZIF-1 is monoclinic, ZIF-2 is orthorhombic whereas ZIF-3 and ZIF-10 have tetragonal structures.[41] ZIF-1 (ZIF-2) has 6.9 Å pores in diameter with 3 Å (6 Å) pore apertures.[42] ZIF-3 (ZIF-10) has 6 Å (12.1 Å) pores in diameter with 4.6 Å (8.2 Å) pore apertures.[41,42] $Zn(bdc)(ted)_{0.5}$ and bioMOF-11 were chosen to represent MOFs with smaller pores. $Zn(bdc)(ted)_{0.5}$ is a tetragonal structure with one channel having cross section of 7.5 Å × 7.5 Å and a smaller channel with a cross section of 4.8 Å × 3.2 Å.[43] BioMOF-11 has a tetragonal structure, and each cavity in the structure can accommodate a sphere with a diameter of 5.8 Å; the aperture of cavities is 5.2 Å.[44] The experimental gas adsorption data for noble gases in MOFs is Xe adsorption in IRMOF-1 and Xe, Kr adsorption in CPO-27-Ni. We considered these MOFs in this study to validate the accuracy of force field parameters by comparing the predictions of molecular simulations with the available experimental data.

The atomic positions of all MOFs were obtained from their experimental XRD data, and rigid structures were used. We compared the results of molecular simulations using rigid and flexible force fields for Xe adsorption in the next section. The Dreiding[45] force field was used in all simulations to describe the atoms of the MOFs. For the metal atoms, the van der Waals parameters were taken from the Universal Force Field (UFF)[46] since they are not available in the Dreiding force field. Simulation results employing Dreiding force field agreed well with the available experimental data for single component adsorption isotherms of Xe in IRMOF-1 and Xe and Kr in CPO-27-Ni (see Figure 1).

Spherical Lennard-Jones (LJ) 12−6 potentials were used to model Xe (ε/k_B = 221 K, σ = 4.01 Å), Kr (ε/k_B = 166.4 K, σ = 3.636 Å), and Ar (ε/k_B = 119.8 K, σ = 3.4 Å).[26,47] The Lorentz−Berthelot mixing rules were employed to calculate the adsorbate−adsorbent and adsorbate−adsorbate LJ cross interaction parameters. The intermolecular potentials were truncated at 13 Å for adsorption and diffusion simulations. A minimum 2 × 2 × 2 unit cell simulation box was used for GCMC simulations. For EMD simulations, the size of the simulation box was increased up to 3 × 3 × 3 to contain enough particles at the lowest loadings. Periodic boundary conditions were applied in all simulations.[48,49] Conventional GCMC was employed to compute the single component and

dx.doi.org/10.1021/ie300766s | Ind. Eng. Chem. Res. 2012, 51, 7373−7382

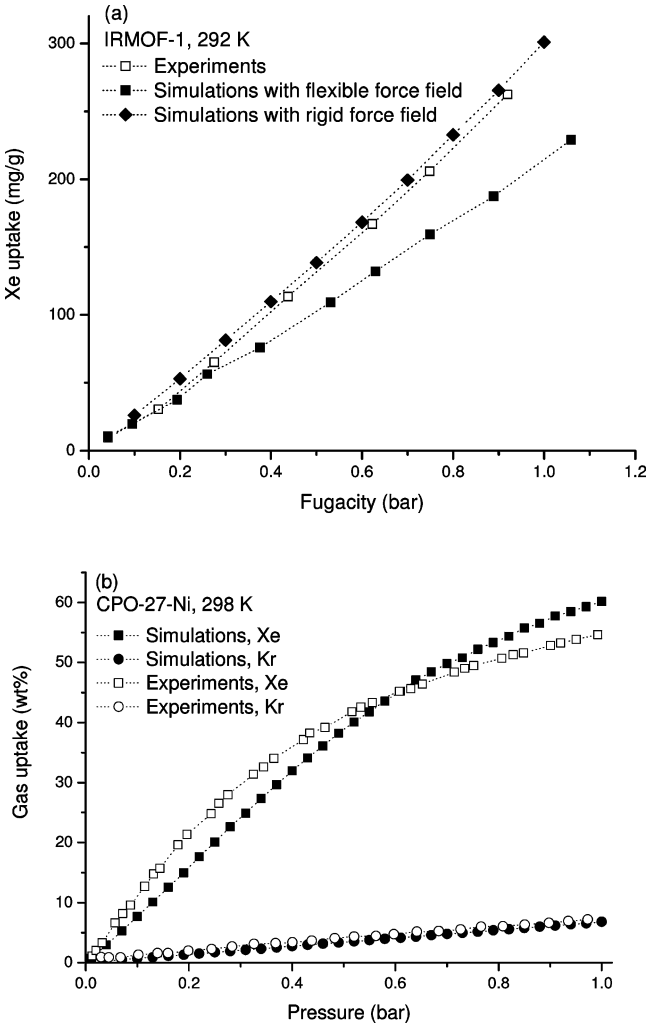

Figure 1. Experimental and simulated adsorption isotherms of (a) Xe in IRMOF-1 and (b)Xe and Kr in CPO-27-Ni. Experimental data was taken from the work of (a) Greathouse et al.[25] and (b) Thallapally et al.[27]

**fugacity, effective partial pressure

mixture adsorption isotherms of gases. The temperature and the fugacity of the adsorbing gases were specified and the number of adsorbed molecules was calculated at equilibrium. Simulations at the lowest fugacity for each system were started from an empty MOF matrix. Each subsequent simulation at higher fugacity was started from the final configuration of the previous run. Simulations consisted of a total of 3×10^7 trial configurations with the last half of the configurations used for data collection. A configuration is defined as an attempted translation, or creation or deletion, of the adsorbates. For the case of mixture simulations, there is also an attempted swap of the particle species.

A good indication of the ability for separation in an equilibrium-based separation process is the adsorption selectivity of a nanoporous material for different components in the mixtures. The adsorption selectivity of MOFs for Xe from Xe/Kr and Xe/Ar mixtures was defined as

$$S_{\text{adsorption}_{(\text{Xe/Kr})}} = \frac{x_{\text{Xe}}/x_{\text{Kr}}}{y_{\text{Xe}}/y_{\text{Kr}}} \tag{1a}$$

$$S_{\text{adsorption}_{(\text{Xe/Ar})}} = \frac{x_{\text{Xe}}/x_{\text{Ar}}}{y_{\text{Xe}}/y_{\text{Ar}}} \tag{1b}$$

where x and y are the molar fractions of the adsorbed and bulk phases, respectively. As discussed in previous studies,[9] adsorption selectivity and working capacity (also known as delta loading) govern the costs of separation in adsorption-based separation processes. Using GCMC simulations, the Xe working capacities of the MOFs were calculated as the difference in gas uptakes at a total gas phase fugacity of 10 bar and a desorption pressure of 1 bar at room temperature.

Single component and mixture self-diffusivities of each species were calculated using EMD simulations. The details of using EMD simulations to obtain self-diffusion coefficients have been described in previous studies of zeolites, carbon nanotubes, and MOFs.[50−53] The self-diffusivity, $D_{\text{self},i}$ describes the motion of individual tagged particles, and in an isotropic three-dimensional material, it is related to the mean-squared displacement of tagged particles by the Einstein relation,

$$D_{\text{self},i} = \lim_{t\to\infty} \frac{1}{6t} \left\langle \frac{1}{N_t} \sum_{l=1}^{N_i} [r_{il}(t) - r_{il}(0)]^2 \right\rangle \tag{2}$$

where N is the number of molecules, $r_{il}(t)$ is the three-dimensional position vector of molecule l of species i at time t, and the angular brackets denote the ensemble average.[54] The self-diffusivities of gases in the pores of MOFs were reported as average diffusivities using $D_{\text{self},i} = (D_{\text{self},x,i} + D_{\text{self},y,i} + D_{\text{self},z,i})/3$. Among the MOFs we considered in this work, CPO-27-Ni and CPO-27-Co have one-dimensional pores; therefore, self-diffusivities of noble gases in CPOs were reported only in the z direction. The Nosé−Hoover thermostat in the *NVT*-ensemble was used in all EMD simulations. After creating initial states with the appropriate loadings using GCMC simulations, each system was first equilibrated with EMD for about 20 ps prior to taking data. Self-diffusivities of each component were computed at various adsorbed loadings of Xe/Kr and Xe/Ar mixtures that were obtained from mixture GCMC simulations.

Once adsorption and diffusion data of gas mixtures were obtained from detailed molecular simulations as described above, the performance of each MOF as a membrane for Xe/Kr and Xe/Ar separations can be predicted. Previous studies showed that permeation selectivity of a MOF membrane can be approximated as the multiplication of adsorption selectivity and diffusion selectivity:[9,10,55]

$$S_{\text{permeation}_{(\text{Xe/Kr})}} = \frac{x_{\text{Xe}}/x_{\text{Kr}}}{y_{\text{Xe}}/y_{\text{Kr}}} \frac{D_{\text{Xe,self}}(x_{\text{Xe}}, x_{\text{Kr}})}{D_{\text{Kr,self}}(x_{\text{Xe}}, x_{\text{Kr}})} \tag{3a}$$

$$S_{\text{permeation}_{(\text{Xe/Ar})}} = \frac{x_{\text{Xe}}/x_{\text{Ar}}}{y_{\text{Xe}}/y_{\text{Ar}}} \frac{D_{\text{Xe,self}}(x_{\text{Xe}}, x_{\text{Ar}})}{D_{\text{Ar,self}}(x_{\text{Xe}}, x_{\text{Ar}})} \tag{3b}$$

The validation of this approximate expression for MOF membranes was previously showed by Keskin and Sholl.[55] In this approximate expression, the diffusion selectivity is defined as the ratio of self-diffusivities of each gas in a binary mixture evaluated directly at their corresponding adsorbed compositions. Equation approximates a membrane's permeation selectivity at a specified feed pressure and feed gas composition based on a single GCMC simulation and an EMD simulation performed at the loadings determined from this GCMC simulation. We reported the permeation selectivity of MOFs

dx.doi.org/10.1021/ie300766s | Ind. Eng. Chem. Res. 2012, 51, 7373−7382

for Xe/Kr and Xe/Ar separations as a function of feed pressure at room temperature.

High gas selectivity without high gas permeability has limited value for membrane-based gas separations since this type of membranes will require large surface areas, thus high capital costs. In order to assess the performance of MOF membranes in noble gas separations, we computed gas permeabilities using the following expression:[10]

$$P_i = \frac{\phi D_{i,\text{self}} c_i}{f_i} \quad (4)$$

In this expression, P_i is the permeability of species i (mol/(m s Pa)), ϕ is the fractional pore volume of the material, $D_{i,\text{self}}$ is the self-diffusivity of species i in the mixture (m^2/s), c_i is the concentration of species i at the upstream face of the membrane (mol/m^3), and f_i is the bulk phase fugacity of the species i (Pa). A more commonly used unit for reporting permeability in the membrane community is Barrers; therefore, predicted gas permeabilities were reported in Barrers throughout this work.

RESULTS AND DISCUSSION

**validation of initial config.

We first compared the results of our molecular simulations with the available experimental data for adsorption of noble gases in MOFs. Figure 1a shows experimental Xe adsorption isotherm of IRMOF-1 at 292 K, simulated Xe adsorption isotherm by Greathouse et al.[25] using flexible framework, and our simulated Xe adsorption isotherm using rigid framework. Greathouse et al. used the LJ parameters defined by Dubbeldam et al.[56] for IRMOF-1 atoms whereas we used Dreiding force field parameters. There is a very good agreement between experiments and both molecular simulations at low pressures whereas at higher pressures simulations employing rigid force field are in a better agreement with the experimental data. Here it is important to note that using flexible force field is actually a more realistic approach than using rigid force field. The aim of Figure 1a is to show that rigid force field can give as accurate results as flexible force field and save a significant amount of computational time. Thallapally et al.[27] very recently measured single component Xe and Kr adsorption isotherms at room temperature in CPO-27-Ni and activated carbon. Figure 1b shows that our simulation results agree with the experimental data both for Xe and Kr adsorption. The small discrepancy between experimental and simulated isotherms can be attributed to the perfect, defect free crystal structure assumption of the simulations and the accuracy of the force fields. For example, experiments reported Xe uptake of 55.6 wt % at 1 bar, 298 K, and our simulations predicted 59.1 wt % under the same conditions. The uptake capacity of CPO-27-Ni is higher than that of activated carbon which adsorbs 48 wt % Xe at 1 bar, 298 K.

Single component Xe, Kr, and Ar uptake of MOFs at 5 and 10 bar were tabulated in Table 2. We also included the experimental measurements of Bazan et al.[57] for Xe, Kr, and Ar uptake in three zeolites, SorboNorit B3, Koestrolith 13X-K2, and Koestrolith 4AK. The comparison between zeolites and MOFs showed that MOFs considered in this work exhibit higher Xe, Kr, and Ar uptake capacities than Koestrolith 4AK. All MOFs except bioMOF-11 and ZIF-1 have higher Kr and Ar uptake capacities than Koestrolith 13X-K2 and SorboNorit B3 at 10 bar. These results suggest that MOFs studied in this work can be potential candidates for noble gas storage.

Table 2. Single Component Uptake of Xe, Kr, and Ar in MOFs and Zeolites

	Xe (mmol/g)		Kr (mmol/g)		Ar (mmol/g)	
MOFs (298 K, this work)	5 bar	10 bar	5 bar	10 bar	5 bar	10 bar
BioMOF-11	3.84	3.91	2.44	3.21	0.93	1.62
CuBTC	8.95	10.03	3.95	6.60	1.73	3.03
IRMOF-1	11.45	15.80	2.78	5.57	1.31	2.57
CPO-27-Co	7.12	7.92	3.67	5.78	1.29	2.40
CPO-27-Ni	6.73	7.34	3.45	5.38	1.25	2.29
ZIF-1	2.68	2.83	2.39	2.87	1.23	1.84
ZIF-2	6.12	6.60	4.36	5.80	1.83	3.08
ZIF-3	8.08	8.79	3.79	5.69	1.59	2.70
ZIF-10	8.26	9.63	2.64	4.72	1.09	2.07
$Zn(bdc)(ted)_{0.5}$	8.47	8.93	5.51	7.35	2.11	3.67
zeolites (303 K, Bazan et al.[57])						
SorboNorit B3	5.58		2.8	3.79	0.95	1.70
Koestrolith 13X-K2	9.18	9.83	2.58	4.00	0.44	0.73
Koestrolith 4AK	~1.60		1.17	1.66	0.41	0.72

Single-component adsorption isotherms of Xe, Kr, and Ar and binary adsorption isotherms of Xe/Kr and Xe/Ar mixtures in all MOFs at 298 K are shown in Figures S1 and S2 of the Supporting Information. As representatives, adsorption isotherms of CPO-27-Ni, ZIF-3, and $Zn(bdc)(ted)_{0.5}$ were given in Figure 2. Adsorption of Xe is higher than that of Kr and Ar in all MOFs due to energetic effects. As the pressure increases, Xe reaches saturation whereas smaller Kr atoms can still find places in the narrow pores of bioMOF-11, CuBTC, ZIF-2, and $Zn(bdc)(ted)_{0.5}$. Therefore, Kr adsorption gets higher than Xe at higher pressures in these materials due to entropic effects. As should be expected from the single component isotherms, mixture GCMC simulations showed that adsorption favors Xe over Kr and Ar in the mixtures because the more strongly adsorbing Xe atoms exclude the weakly adsorbed ones in the pores.

We used Ideal Adsorbed Solution Theory (IAST)[58] to determine whether pure adsorption isotherms could be used to make accurate predictions for mixture isotherms. IAST is well-known to give accurate predictions for mixture adsorption isotherms based on adsorption isotherms of pure gases in many nanoporous materials except in materials characterized by strong energetic or geometric heterogeneity.[59,60] In order to apply IAST, we fitted dual-site Langmuir and dual-site Freundlich models to single component adsorption isotherms of Xe, Kr, and Ar. The single component isotherm fits and the predictions of IAST were shown in Figure 2 by continuous lines and dotted lines, respectively. The predictions of IAST agree fairly well with the mixture GCMC simulations of MOFs.

After mixture adsorption data was obtained using GCMC simulations, we estimated the performances of MOFs in adsorption-based noble gas separation applications. The adsorption selectivities of MOFs as a function of Xe composition in the bulk phase at 1 and 10 bar for Xe/Kr and Xe/Ar mixtures are shown in Figures S3 and S4 of the Supporting Information. Our values for Xe/Kr selectivity of IRMOF-1 (3.5−4.3) agreed well with the previous results of Ryan et al.,[26] and our values for Xe/Ar selectivity of IRMOF-1 (7−11.2) agreed with the previous results of Greathouse et al.[25] MOFs having small pores such as bioMOF-11, $Zn(bdc)(ted)_{0.5}$, ZIF-1, ZIF-2, and CuBTC exhibit higher adsorption selectivities (7−16 for Xe/Kr and 19−79 for Xe/Ar) than MOFs having

dx.doi.org/10.1021/ie300766s | Ind. Eng. Chem. Res. 2012, 51, 7373−7382

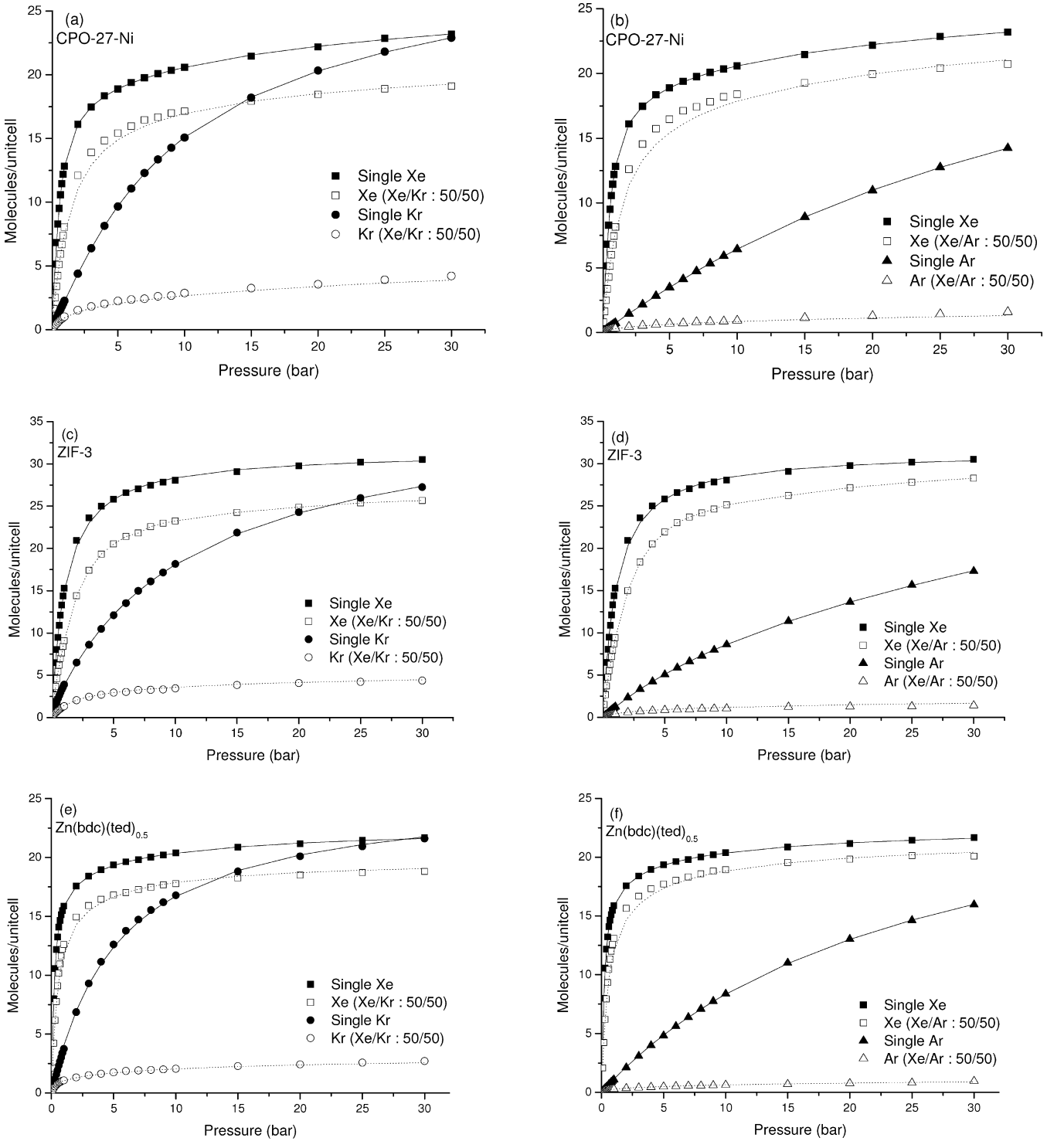

Figure 2. Single-component and binary adsorption isotherms of Xe/Kr and Xe/Ar in (a and b) CPO-27-Ni, (c and d) ZIF-3, and (e and f) $Zn(bdc)(ted)_{0.5}$ at room temperature. The composition of the bulk gas mixture is equimolar. The continuous and dotted lines represent the fitted single component adsorption isotherm and the prediction of IAST, respectively.

large pores such as IRMOF-1, CPO-27-Ni, and CPO-Co (3−8 for Xe/Kr and 7−28 for Xe/Ar). This can be explained with the following discussion: Materials with relatively smaller pores provide a stronger confinement for Xe atoms whereas the degree of confinement of Kr or Ar atoms in small pores and large pores can be thought as being similar, because in both cases the atom is small relative to the pore size, giving similar adsorption strength. The stronger confinement of Xe in narrow-pore MOFs results in higher adsorption selectivity for Xe.

Figure 3 shows that Xe selectivity from Xe/Ar mixtures is higher than the one from Xe/Kr mixtures. The adsorption selectivity was greatly enhanced when Xe was mixed with smaller atoms (Ar) compared to the larger atoms (Kr). For example, at 1 bar, ZIF-2 (ZIF-10) exhibits Xe selectivity of ∼10 and ∼40 (∼5 and ∼15) from equimolar Xe/Kr and Xe/Ar

dx.doi.org/10.1021/ie300766s | Ind. Eng. Chem. Res. 2012, 51, 7373−7382

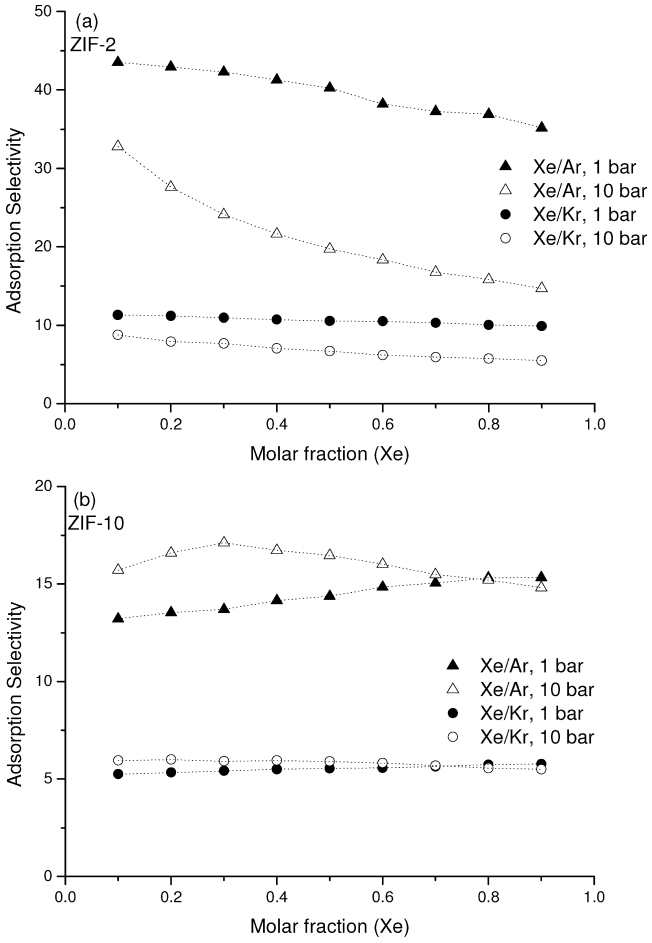

Figure 3. Effect of feed gas composition and pressure on Xe selectivity for Xe/Kr and Xe/Ar separations.

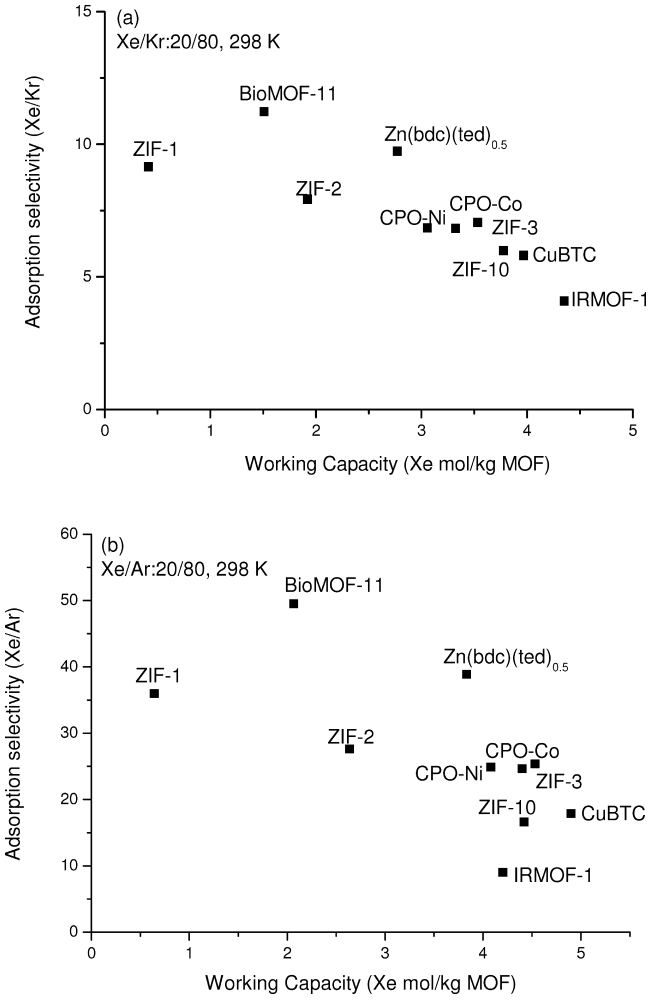

Figure 4. Adsorption selectivity and working capacity of MOFs for (a)Xe/Kr and (b)Xe/Ar separations.

mixtures, respectively. The effect of feed gas composition on the adsorption selectivity can be also seen in Figures 3, S3, and S4 (of the Supporting Information). As the composition of Xe in the feed increases, the adsorbed amount of Xe (Kr or Ar) increases (decreases). The selectivities of ZIF-2 and ZIF-10 shown in Figure 3 are largely independent of the feed composition of Xe at 1 bar. As discussed in previous studies,[12,25] adsorbate−adsorbate interactions become more dominant at 10 bar and Xe selectivity becomes composition dependent at this pressure.

Maintaining the selectivity across a wide range of pressures is also desired for an adsorption-based separation process. Figures S3 and S4 of the Supporting Information show that materials having small pores/pockets exhibit high adsorption selectivities at 1 bar but this selectivity drops off quickly at 10 bar. For example, Xe is strongly confined in the narrow pores of CuBTC, $Zn(bdc)(ted)_{0.5}$, ZIF-1, and ZIF-2, and these MOFs exhibit high Xe selectivity over Kr and Ar at 1 bar. However, as pressure is increased to 10 bar, small pockets are filled and adsorbates go into the large cavities of the MOFs; hence, Xe selectivity decreases. This result suggests that MOFs with uniformly small pores without large cavities can be better candidates for noble gas separations.

Figure 4 compares the adsorption selectivities and working capacities of MOFs. The adsorption selectivities and working capacities were calculated for Xe/Kr:20/80 mixtures to represent an industrial gas mixture.[61] The most desirable materials for adsorption-based separation of noble gases should be located in the top right-hand corner of Figure 4. The results of molecular simulations showed that there is a trade-off between adsorption selectivity and working capacity. For example, ZIF-1 exhibits good Xe/Kr selectivity (∼9) but low Xe working capacity (∼0.41 mol Xe/kg MOF) whereas IRMOF-1 has a high working capacity (∼4.35 mol Xe/kg MOF) but low selectivity (∼4). Among the MOFs studied in this work, $Zn(bdc)(ted)_{0.5}$ can be considered as the material with the best Xe selectivity/working capacity combination (10 and 2.77 mol Xe/kg MOF, respectively). It is also important to compare the separation performance of MOFs with that of well-known zeolites. Previous research showed that NaX zeolite has a selectivity of ∼6 for Xe over Kr.[26,62] NaA zeolite has a Xe selectivity of 4−4.5 (20−25) from an equimolar Xe/Kr (Xe/Ar) mixture at 300 K between 1 and 10 bar.[63] Except IRMOF-1 and ZIF-10 all the MOFs considered in this work show higher Xe selectivity than NaA and NaX. For example, under the same conditions, $Zn(bdc)(ted)_{0.5}$ has a Xe selectivity of 10−12.5 (30−50) for Xe/Kr (Xe/Ar) separations.

The transport rates of gas components inside the material of interest are crucial in determining the overall performance of this material in gas separation applications. We computed self-diffusivities of Xe/Kr and Xe/Ar mixtures in MOFs using EMD simulations. As expected, strongly adsorbed component diffuses

dx.doi.org/10.1021/ie300766s | Ind. Eng. Chem. Res. 2012, 51, 7373−7382

slowly compared to the weakly adsorbed component. For example, room temperature self-diffusivities of Xe and Kr (Ar) in Xe/Kr:20/80 (Xe/Ar:20/80) mixtures in IRMOF-1 were 5.7 × 10^{-5} and 1.2 × 10^{-4} (2.3 × 10^{-4}) cm^2/s, respectively. Our diffusivity data agreed well with the previously reported Ar diffusion in IRMOF-1.[52] The self-diffusivities of Xe were computed as 1−5 × 10^{-5} cm^2/s in $Zn(bdc)(ted)_{0.5}$, IRMOF-1, and ZIFs and ∼10^{-4} cm^2/s in CPOs. These diffusivities are comparable with the ones in carbon nanotubes and zeolites. Nasrabadi et al.[64] recently used EMD simulations and calculated self-diffusivities of Xe and Kr (Ar) in a (10,10) single walled carbon nanotube at 300 K as 7.5 × 10^{-6} and 1.7 × 10^{-5} (3.4 × 10^{-5}) cm^2/s. Bergh et al.[65] reported self-diffusivity of Ar using EMD simulations in DDR, CHA, FAU, and MFI as 1−2 × 10^{-5}, 3 × 10^{-5}, 4 × 10^{-5}, and 0.5−2 × 10^{-4} cm^2/s, respectively. Luca et al.[66] reported calculated and experimental diffusivities of Ar and Xe as 2−3.1 × 10^{-6} and 2.7−2.8 × 10^{-5} cm^2/s in silicalite-1 at 300 K.

Using adsorption and diffusion selectivities calculated from GCMC and EMD simulations, we estimated permeation selectivities of MOFs for Xe/Kr and Xe/Ar mixtures. In Figure 5, the selectivity greater than 1 indicates that MOF is selective for Xe. As discussed before, adsorption selectivity favors Xe due to energetic effects but it was compensated by the low diffusion selectivities toward Xe since strongly adsorbed Xe species diffuse more slowly than the weakly adsorbed species. As a result, permeation selectivities of MOFs for Xe are smaller than their adsorption selectivities. As an example, adsorption selectivity of bioMOF-11 for Xe/Kr mixture is 11 at 10 bar, 298 K whereas diffusion selectivity is 0.6 indicating that Kr diffuses 1.6 times faster than Xe in the pores of bioMOF-11. The combined effect of adsorption and diffusion preferences resulted in Xe selective bioMOF-11 membrane with a selectivity of 6.6.

Figure 6 compares permeation selectivity and permeability of MOFs for Xe/Kr and Xe/Ar separations at a feed pressure of 10 bar. The most desirable materials for permeation-based separation of noble gases should have both high permeation selectivity and high permeability. High permeability is desired to perform the separation with a smaller membrane area, thus low capital cost. Figure 6 shows that CPOs having one-dimensional large pores in z direction exhibit higher Xe permeability than all other MOFs. This can be attributed to the high adsorption and fast diffusion of Xe in CPOs (17 molecules per unit cell and 10^{-4} cm^2/s at 10 bar, 298 K). Figure 6b shows that Xe permability of CPO-27-Co is slightly higher than that of CPO-27-Ni which can be attributed to the stronger confinement of Xe atoms in the former due to the larger kinetic

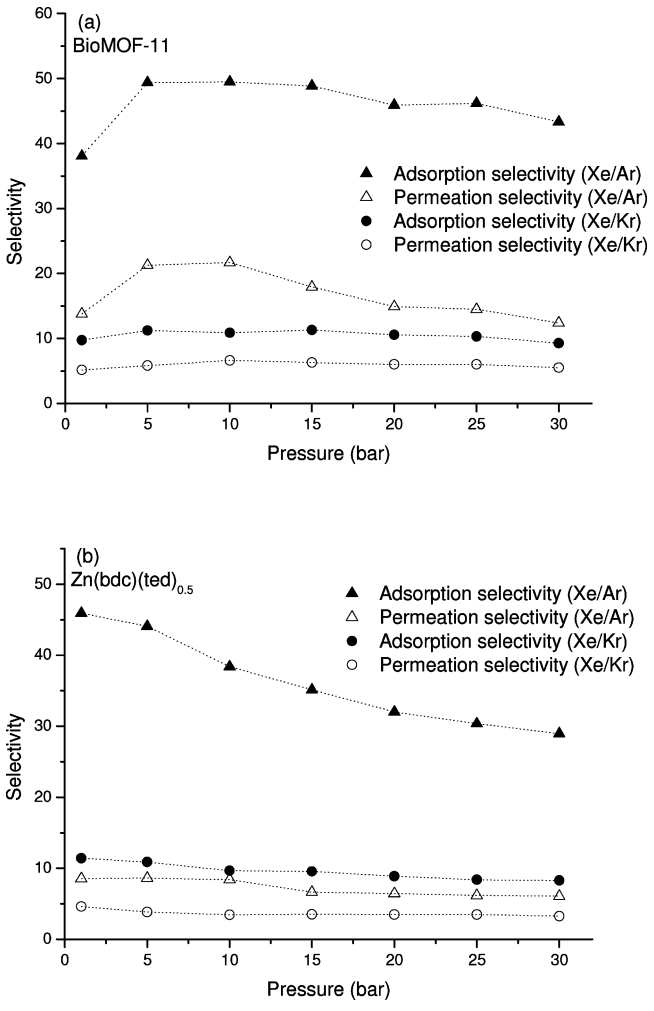

Figure 5. Adsorption and permeation selectivity of MOFs at 298 K as a function of pressure. The composition of the bulk gas mixture is 20/80.

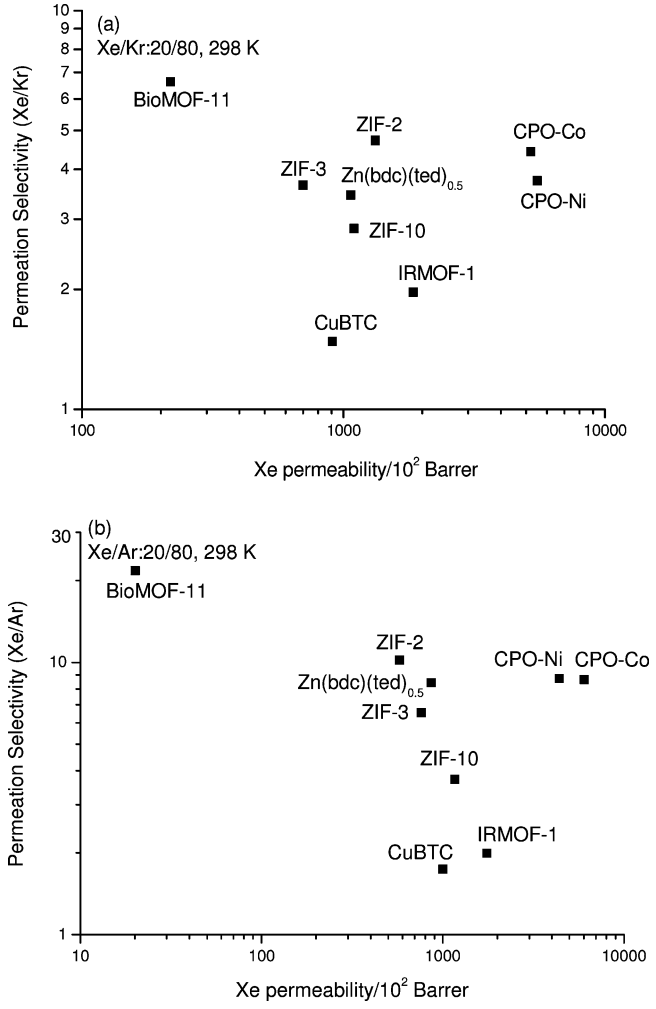

Figure 6. Permeation selectivity and gas permeability of MOFs at 10 bar for (a) Xe/Kr and (b) Xe/Ar separations.

dx.doi.org/10.1021/ie300766s | Ind. Eng. Chem. Res. 2012, 51, 7373−7382

diameter of Co atoms that constrains the pores. Since both adsorption and diffusion selectivities of CPOs for Xe/Ar mixtures are close to each other (~25 and ~0.35, respectively), it is expected to see similar Xe/Ar permeation selectivities (~8.7) for these two materials. The diffusivity of Xe in bioMOF-11 is low ($6-8 \times 10^{-7}$ cm^2/s); therefore, the permeability of this MOF is lower than the other MOFs. It is important to compare the noble gas permeability of MOF membranes with other nanoporous membranes to assess the performance of MOFs in noble gas separations. Sholl[67] computed single-component steady state permeance of Xe through a 10 μm thick $AlPO_4$-31 single crystal membrane as 10^{-5} mol/(m^2 s Pa) at 300 K. Our calculated Xe permeances were $7.3 \times 10^{-7}-1.8 \times 10^{-5}$ mol/(m^2 s Pa) at 298 K for Xe/Kr:20/80 bulk gas mixtures in 10 μm thick MOF membranes. Nakai et al.[68] measured permeability of Xe in cellulose acetate membranes as 0.97−2.7 barrers whereas we calculated Xe permeabilities in a range of 2−55 barrers in MOFs. Considering the porosity of MOFs, it is natural to observe higher gas permeabilities in MOF membranes compared to polymer membranes.

■ CONCLUSIONS

We used GCMC and EMD simulations to assess the adsorption-based and permeation-based separation performances of various MOFs for Xe/Kr and Xe/Ar separations. Results showed that bioMOF-11, $Zn(bdc)(ted)_{0.5}$, ZIF-1, and ZIF-2 have the highest adsorption selectivities for Xe/Kr and Xe/Ar separations. This was attributed to narrow pore-strong confinement characteristics of these materials. A trade-off was observed between adsorption-based selectivity and working capacity. Large pore materials with low adsorption selectivities such as IRMOF-1 exhibited high working capacities. We estimated permeation selectivities and gas permeabilities of MOFs by computing self-diffusivities and adsorption isotherms of each component in the mixture and concluded that MOFs examined in this study can be better membrane materials than zeolites.

■ ASSOCIATED CONTENT

Ⓢ Supporting Information

Adsorption isotherms for single component and binary mixtures of Xe, Kr, and Ar in MOFs, adsorption selectivity of MOFs for Xe/Kr and Xe/Ar mixtures as a function of gas composition, and adsorption and permeation selectivity of MOFs as a function of pressure for Xe/Kr and Xe/Ar mixtures. This material is available free of charge via the Internet at http://pubs.acs.org.

■ AUTHOR INFORMATION

Corresponding Author

*E-mail: skeskin@ku.edu.tr.

Notes

The authors declare no competing financial interest.

■ REFERENCES

(1) James, S. J. Metal Organic Frameworks. *Chem. Soc. Rev.* **2003**, *32*, 276.
(2) Rowsell, J. L. C.; Yaghi, O. M. Metal-Organic Frameworks: A New Class of Porous Materials. *Microporous Mesoporous Mater.* **2004**, *73*, 3.
(3) Uemura, K.; Matsuda, R.; Kitagawa, S. Flexible Microporous Coordination Polymers. *J. Solid State Chem.* **2005**, *178*, 2420.
(4) Mueller, U.; Schubert, M.; Teich, F.; Puetter, H.; Schierle-Arndt, K.; Pastré, J. Metal Organic Frameworks-Prospective Industrial Applications. *J. Mater. Chem.* **2006**, *16*, 626.
(5) Isaeva, V. I.; Kustov, L. M. Metal Organic Frameworks: New Materials for Hydrogen Storage. *Russ. J. Gen. Chem.* **2007**, *77*, 721.
(6) Düren, T.; Bae, Y. S.; Snurr, R. Q. Using Molecular Simulation to Characterize Metal Organic Frameworks for Adsorption Applications. *Chem. Soc. Rev.* **2009**, *38*, 1237.
(7) Haldoupis, E.; Nair, S.; Sholl, D. S. Efficient Calculation of Diffusion Limitations in Metal Organic Framework Materials:A Tool for Identifying Materials for Kinetic Separations. *J. Am. Chem. Soc.* **2010**, *132*, 7528.
(8) Han, S. S.; Mendoza-Cortes, J. L.; Goddard, W. A., III Recent Advances on Simulation and Theory of Hydrogen Storage in Metal Organic Frameworks and Covalent Organic Frameworks. *Chem. Soc. Rev.* **2009**, *38*, 1460.
(9) Krishna, R.; van Baten, J. M. In Silico Screening of Metal-Organic Frameworks in Separation Applications. *Phys. Chem. Chem. Phys.* **2011**, *13*, 10593.
(10) Krishna, R.; van Baten, J. M. In Silica Screening of Zeolite Membranes for CO_2 Capture. *J. Membr. Sci.* **2010**, *360*, 323.
(11) Liu, Y. H.; Liu, D. H.; Yang, Q. Y.; Mi, J. G.; Zhong, C. L. Comparative Study of Separation Performance of COFs and MOFs for $CH_4/CO_2/H_2$ Mixtures. *Ind. Eng. Chem. Res.* **2010**, *49*, 2902.
(12) Yang, Q.; Chunyu, X.; Zhong, C.; Chen, J.-F. Molecular Simulation of Separation of CO_2 from Flue Gases in Cu-Btc Metal-Organic Framework. *AIChE J.* **2007**, *53*, 2832.
(13) Guo, H.; Shi, F.; Ma, Z.; Liu, X. Molecular Simulation for Adsorption and Separation of CH_4/H_2 in Zeolitic Imidazolate Frameworks. *J. Phys. Chem. C* **2010**, *114*, 12158.
(14) Nalaparaju, A.; Zhao, X. S.; Jiang, J. W. Molecular Understanding for the Adsorption of Water and Alcohols in Hydrophilic and Hydrophobic Zeolitic Metal Organic Frameworks. *J. Phys. Chem. C* **2010**, *114*, 11542.
(15) Chen, Y.; Jiang, J. A Bio-Metal−Organic Framework for Highly Selective CO_2 Capture: A Molecular Simulation Study. *ChemSusChem* **2010**, *3*, 982.
(16) Zheng, C. C.; Liu, D. H.; Yang, Q. Y.; Zhong, C. L.; Mi, J. G. Computational Study on the Influences of Framework Charges on CO_2 Uptake in Metal-Organic Frameworks. *Ind. Eng. Chem. Res.* **2009**, *48*, 10479.
(17) Babarao, R.; Jiang, J. W.; Sandler, S. I. Molecular Simulations for Adsorptive Separation of CO_2/CH_4 Mixture in Metal-Exposed, Catenated, and Charged Metal-Organic Frameworks. *Langmuir* **2009**, *25*, 6590.
(18) Babarao, R.; Jiang, J. W. Unprecedentedly High Selective Adsorption of Gas Mixtures in Rho Zeolite-Like Metal-Organic Framework: A Molecular Simulation Study. *J. Am. Chem. Soc.* **2009**, *131*, 11417.
(19) Atci, E.; Erucar, I.; Keskin, S. Adsorption and Transport of CH_4, CO_2, H_2 Mixtures in a Bio-MOF Material from Molecular Simulations. *J. Phys. Chem. C* **2011**, *115*, 6833.
(20) Atci, E.; Keskin, S. Atomically Detailed Models for Transport of Gas Mixtures in ZIF Membranes and ZIF/Polymer Composite Membranes. *Ind. Eng. Chem. Res.* **2012**, *51*, 3091.
(21) Keskin, S. Comparing Performance of CPO and IRMOF Membranes for Gas Separations Using Atomistic Models. *Ind. Eng. Chem. Res.* **2010**, *48*, 11689.
(22) Keskin, S. Atomistic Simulations for Adsorption, Diffusion, and Separation of Gas Mixtures in Zeolite Imidazolate Frameworks. *J. Phys. Chem. C* **2011**, *115*, 800.
(23) Keskin, S.; Sholl, D. S. Assessment of a Metal-Organic Framework Membrane for Gas Separations Using Atomically Detailed Calculations: CO_2, CH_4, N_2, H_2 Mixtures in MOF-5. *Ind. Eng. Chem. Res.* **2009**, *48*, 914.
(24) Keskin, S. Adsorption, Diffusion and Separation of CH_4/H_2 Mixtures in Covalent Organic Frameworks: Molecular Simulations and Theoretical Predictions. *J. Phys. Chem. C* **2012**, *116*, 1772.

(25) Greathouse, J. A.; Kinnibrugh, T. L.; Allendorf, M. D. Adsorption and Separation of Noble Gases by IRMOF-1: Grand Canonical Monte Carlo Simulations. *Ind. Eng. Chem. Res.* **2009**, *48*, 3425.
(26) Ryan, P.; Farha, O. K.; Broadbelt, L. J.; Snurr, R. Q. Computational Screening of Metal-Organic Frameworks for Xenon/Krypton Separation. *AIChE J.* **2011**, *57*, 1759.
(27) Thallapally, P. K.; Grate, J. W.; Motkuri, R. K. Facile Xenon Capture and Release at Room Temperature Using a Metal-Organic Framework: A Comparison with Activated Charcoal. *Chem. Commun.* **2012**, *48*, 347.
(28) Hoffmann, H. C.; Assfour, B.; Epperlein, F.; Klein, N.; Paasch, S.; Senkovska, I.; Kaskel, S.; Seifert, G.; Brunner, E. High-Pressure in Situ (129)Xe NMR Spectroscopy and Computer Simulations of Breathing Transitions in the Metal-Organic Framework Ni(2)(2,6-Ndc)(2)(Dabco) (Dut-8(Ni). *J. Am. Chem. Soc.* **2011**, *133*, 8681.
(29) Eddaoudi, M.; Kim, J.; Rosi, N.; Vodak, D.; Wachter, J.; O'Keeffe, M.; Yaghi, O. M. Systematic Design of Pore Size and Functionality in Isoreticular MOFs and Their Application in Methane Storage. *Science* **2002**, *295*, 469.
(30) Greathouse, J. A.; Allendorf, M. D. Force Field Validation for Molecular Dynamics Simulations of IRMOF-1 and Other Isoreticular Zinc Carboxylate Coordination Polymers. *J. Phys. Chem. C* **2008**, *112*, 5795.
(31) Babarao, R.; Jiang, J. Diffusion and Separation of CO_2 and CH_4 in Silicalite, C_{168} Schwarzite and IRMOF-1: A Comparative Study from Molecular Dynamics Simulation. *Langmuir* **2008**, *24*, 5474.
(32) Dubbeldam, D.; Frost, H.; Walton, K. S.; Snurr, R. Q. Molecular Simulation of Adsorption Sites of Light Gases in the Metal-Organic Framework IRMOF-1. *Fluid Phase Equilib.* **2007**, *261*, 152.
(33) Babarao, R.; Hu, Z.; Jiang, J.; Chempath, S.; Sandler, S. I. Storage and Separation of CO_2 and CH_4 in Silicalite, C168 Schwarzite, and IRMOF-1: A Comparative Study from Monte Carlo Simulations. *Langmuir* **2007**, *23*, 659.
(34) Chui, S. S.-Y.; Lo, S. M.-F.; Charmant, J. P. H.; Orpen, A. G.; Williams, I. D. A Chemically Functionalizable Nanoporous Material $[Cu_3(Tma)_2(H_2o)_3]_N$. *Science* **1999**, *283*, 1148.
(35) Keskin, S.; Liu, J.; Johnson, J. K.; Sholl, D. S. Atomically-Detailed Models of Gas Mixture Diffusion through CuBTC Membranes. *Microporous Mesoporous Mater.* **2009**, *125*, 101.
(36) Chmelik, C.; Kärger, J.; Wiebcke, M.; Caro, J.; van Baten, J. M.; Krishna, R. Adsorption and Diffusion of Alkanes in CuBTC Crystals Investigated Using Infra-Red Microscopy and Molecular Simulations. *Microporous Mesoporous Mater.* **2009**, *117*, 22.
(37) Rosi, N. L.; Kim, J.; Eddaoudi, M.; Chen, B. L.; O'Keeffe, M.; Yaghi, O. M. Rod Packings and Metal-Organic Frameworks Constructed from Rod-Shaped Secondary Building Units. *J. Am. Chem. Soc.* **2005**, *127*, 1504.
(38) Dietzel, P. D. C.; Panella, B.; Hirscher, M.; Blom, R.; Fjellvag, H. Hydrogen Adsorption in a Nickel Based Coordination Polymer with Open Metal Sites in the Cylindrical Cavities of the Desolvated Framework. *Chem. Commun.* **2006**, 959.
(39) Park, K. S.; Ni, Z.; Cote, A. P.; Choi, J. Y.; Huang, R. D.; Uribe-Romo, F. J.; Chae, H. K.; O'Keeffe, M.; Yaghi, O. M. Exceptional Chemical and Thermal Stability of Zeolitic Imidazolate Frameworks. *Proc. Natl. Acad. Sci. U.S.A.* **2006**, *103*, 10186.
(40) Hayashi, H.; Cote, A. P.; Furukawa, H.; O'Keeffe, M.; Yaghi, O. M. Zeolite A Imidazolate Frameworks. *Nat. Mater.* **2007**, *6*, 501.
(41) Phan, A.; Doonan, C. J.; Uribe-Romo, F. J.; Knobler, C. B.; O'Keeffe, M.; Yaghi, O. M. Synthesis, Structure, and Carbon Dioxide Capture Properties of Zeolitic Imidazolate Frameworks. *Acc. Chem. Res.* **2010**, *43*, 58.
(42) Park, K. S.; Ni, Z.; Cote, A. P.; Choi, J. Y.; Huang, R. D.; Uribe-Romo, F. J.; Chae, H. K.; O'Keeffe, M.; Yaghi, O. M. Exceptional Chemical and Thermal Stability of Zeolitic Imidazolate Frameworks. *Proc. Natl. Acad. Sci. U.S.A.* **2006**, *103*, 10186.
(43) Liu, J.; Lee, J. Y.; Pan, L.; Obermyer, R. T.; Simizu, S.; Zande, B.; Li, J.; Sankar, S. G.; Johnson, J. K. Adsorption and Diffusion of Hydrogen in a New Metal Organic Framework Material:[Zn(Bdc)-$(Ted)_{0.5}$]. *J. Phys. Chem. C* **2008**, *112*, 2911.
(44) An, J.; Geib, S. J.; Rosi, N. L. High and Selective CO_2 Uptake in a Cobalt Adeninate Metal-Organic Framework Exhibiting Pyrimidine- and Amino-Decorated Pores. *J. Am. Chem. Soc.* **2010**, *132*, 38.
(45) Mayo, S. L.; Olafson, B. D.; Goddard, W. A. Dreiding: A Generic Force Field for Molecular Simulations. *J. Phys. Chem. C* **1990**, *94*, 8897.
(46) Rappe, A. K.; Casewit, C. J.; Colwell, K. S.; Goddard, W. A.; Skiff, W. M. UFF, a Full Periodic Table Force Field for Molecular Mechanics and Molecular Dynamics Simulations. *J. Am. Chem. Soc.* **1992**, *114*, 10024.
(47) Maitland, G. C.; Rigby, M.; Smith, E. B.; Wakeham, W. A. *Intermolecular Forces: Their Origin and Determination*; Clarendon Press: Oxford, 1981.
(48) Allen, M. P.; Tildesley, D. J. *Computer Simulation of Liquids*; Clarendon Press;Oxford University Press: Oxford England, New York, 1987.
(49) Frenkel, D.; Smit, B. Understanding Molecular Simulation: From Algorithms to Applications. *Understanding Molecular Simulation:From Algorithms to Applications*; Academic Press: San Diego, 2002.
(50) Ackerman, D. M.; Skoulidas, A. I.; Sholl, D. S.; Johnson, J. K. Diffusivities of Ar and Ne in Carbon Nanotubes. *Mol. Simul.* **2003**, *29*, 677.
(51) Sanborn, M. J.; Snurr, R. Q. Diffusion of Binary Mixtures of CF_4 and N-Alkanes in Faujasite. *Sep. Purif. Technol.* **2000**, *20*, 1.
(52) Skoulidas, A. I.; Sholl, D. S. Self-Diffusion and Transport Diffusion of Light Gases in Metal-Organic Framework Materials Assessed Using Molecular Dynamics Simulations. *J. Phys. Chem. B* **2005**, *109*, 15760.
(53) Skoulidas, A. I.; Sholl, D. S. Molecular Dynamics Simulations of Self-Diffusivities, Corrected Diffusivities, and Transport Diffusivities of Light Gases in Four Silica Zeolites to Assess Influences of Pore Shape and Connectivity. *J. Phys. Chem. A* **2003**, *107*, 10132.
(54) Keil, F. J.; Krishna, R.; Coppens, M. O. Modeling of Diffusion in Zeolites. *Rev. Chem. Eng.* **2000**, *16*, 71.
(55) Keskin, S.; Sholl, D. S. Efficient Methods for Screening of Metal Organic Framework Membranes for Gas Separations Using Atomically-Detailed Models. *Langmuir* **2009**, *25*, 11786.
(56) Dubbeldam, D.; Walton, K. S.; Ellis, D. E.; Snurr, R. Q. Exceptional Negative Thermal Expansion in Isoreticular Metal-Organic Frameworks. *Angew. Chem., Int. Ed.* **2007**, *46*, 4496.
(57) Bazan, R. E.; Bastos-Neto, M.; Moeller, A.; Dreisbach, F.; Staudt, R. Adsorption Equilibria of O_2, Ar, Kr and Xe on Activated Carbon and Zeolites: Single Component and Mixture Data. *Adsorption* **2011**, *17*, 371.
(58) Myers, A. L.; Prausnitz, J. M. Thermodynamics of Mixed-Gas Adsorption. *AIChE J.* **1965**, *11*, 121.
(59) Chen, H.; Sholl, D. S. Examining the Accuracy of Ideal Adsorbed Solution Theory without Curve-Fitting Using Transition Matrix Monte Carlo Simulations. *Langmuir* **2007**, *23*, 6431.
(60) Keskin, S.; Liu, J.; Johnson, J. K.; Sholl, D. S. Testing the Accuracy of Correlations for Multi-Component Mass Transport of Adsorbed Gases in Metal Organic Frameworks: Diffusion of H_2/CH_4 Mixtures in Cu-Btc. *Langmuir* **2008**, *24*, 8254.
(61) Kerry, F. G. *Industrial Gas Handbook: Gas Separation & Purification*; CRC Press: Boca Raton, FL, 2007.
(62) Izumi, J. In *Handbook of Zeolite Science and Technology*; Auerbach, S. M., Carrado, K., Dutta, P., Eds.; Marcel Dekker: New York, 2003.
(63) Jameson, C. J.; Jameson, A. K.; Lim, H. M. Competitive Adsorption of Xenon and Krypton in Zeolite NaA: Xe-129 Nuclear Magnetic Resonance Studies and Grand Canonical Monte Carlo Simulations. *J. Chem. Phys.* **1997**, *107*, 4364.
(64) Foroutan, M.; Nasrabadi, A. T. Adsorption and Separation of Binary Mixtures of Noble Gases on Single-Walled Carbon Nanotube Bundles. *Phys. E* **2011**, *43*, 851.

(65) van den Bergh, J.; Ban, S. A.; Vlugt, T. J. H.; Kapteijn, F. Diffusion in Zeolites: Extension of the Relevant Site Model to Light Gases and Mixtures Thereof in Zeolites DDR, CHA, MFI and FAU. *Sep. Purif. Tech.* **2010**, *73*, 151.
(66) De Luca, G.; Pullumbi, P.; Barbieri, G.; Fama, A. D.; Bernardo, P.; Drioli, E. Gusev and Suter Calculation of the Diffusion Coefficients of Light Gases in Silicalite-1 Membrane and Silica-Sodalite Zeolite. *Sep. Purif. Tech.* **2004**, *36*, 215.
(67) Sholl, D. S. Predicting Single-Component Permeance through Macroscopic Zeolite Membranes from Atomistic Simulations. *Ind. Eng. Chem. Res.* **2000**, *39*, 3737.
(68) Nakai, Y.; Yoshimizu, H.; Tsujita, Y. Enhanced Gas Permeability of Cellulose Acetate Membranes under Microwave Irradiation. *J. Membr. Sci.* **2005**, *256*, 72.
(69) Wu, D.; Wang, C.; Liu, B.; Liu, D.; Yang, Q.; Zhong, C. Large-Scale Computational Screening of Metal-Organic Frameworks for CH_4/H_2 Separation. *AIChE J.*, DOI 10.1002/aic.12744.